Band offsets and interfacial properties of cubic CdS grown by molecular-beam epitaxy on CdTe(110)

David W. Niles
Max-Planck-Institut für Festkörperforschung, Heisenbergstrasse 1, Postfach 80 06 65, D-7000 Stuttgart 80, Federal Republic of Germany

Hartmut Höchst*
Synchrotron Radiation Center, University of Wisconsin–Madison, 3731 Schneider Drive, Stoughton, Wisconsin 53589-3097
(Received 30 November 1989; revised manuscript received 20 February 1990)

We report on the molecular-beam-epitaxy growth of CdS films on CdTe(110), studied with reflection high-energy electron diffraction (RHEED) and angle-resolved photoemission spectroscopy. The exponential attenuation of the Te 4*d* core-level emission as a function of the CdS film thickness and the persistency of the substratelike RHEED pattern demonstrate that CdS films grow epitaxially in the zinc-blende structure rather than the thermodynamically more favorable hexagonal crystal structure. Core-level intensity and line-shape analysis show that the interface is atomically abrupt and nonreactive. From valence-band photoemission spectra, we find that, compared with CdTe, the CdS Γ_8 valence-band maximum is lower by $\Delta\varepsilon_{VB}=0.65$ eV. Taking the known band gap of cubic CdS (2.42 eV) lets us estimate the Γ_6 conduction-band minimum of CdS to be above that of CdTe by $\Delta\varepsilon_{CB}=0.21$ eV. Our theoretical estimates based on dielectric midgap tight-binding calculations, including the hydrostatic contribution of the $\sim 11\%$ tensile lattice strain in the cubic CdS epilayer, predict a much larger valence-band offset of $\Delta\varepsilon_{VB}=1.19$ eV.

I. INTRODUCTION

Transparent conducting semiconductor (TCS) overlayers are known to significantly improve the conversion efficiency of heterostructure solar cells.[1] Good electrical performance of the device imposes requirements on the window material as well as the interface between the absorber and the window. With regard to the interface, one is interested in a minimum number of gap states that can act as recombination centers, as well as an atomically abrupt and impurity-free transition from one material to the other.

CdS is a promising window material for CdTe-based thin-film heterostructure solar cells.[2] The *n*-type CdS overlayer has a direct band gap of 2.42 eV which increases the absorption length for radiation above the 1.56-eV band gap of CdTe, and raises the conversion efficiency above $\sim 10\%$.[3,4] However, very little is known about the details of the interface region. The thermodynamically stable phase of CdS is the wurtzite structure which has C_{6v} crystal point-group symmetry, but a metastable cubic phase of T_d symmetry can be prepared by epitaxial growth on a cubic substrates.[5]

Measurements of the normal incidence reflection spectra of CdS grown on arsenic terminated GaAs(111) by chemical vapor phase transport indicate good quality epitaxy. A comparison of the reflection data of metastable cubic CdS with those of hexagonal CdS shows that the electronic band structures are very similar, the main difference being a double structured E_1 transition which is otherwise degenerate for cubic CdS. The band gap of cubic zinc-blende CdS, as determined from the lowest reflectivity peak, is only a few meV smaller than that of hexagonal CdS.[6]

The epitaxial growth of cubic CdS on either GaAs or CdTe is complicated by the common problem of lattice mismatch. For the former case, the CdS has a 3.2% larger lattice constant and must grow under considerable compressive strain. For CdTe, however, the lattice constant is larger by $\sim 11\%$ (6.45 Å versus 5.82 Å), and the CdS epilayer must grow under severe tensile strain.[6–8]

Strain modifies the electronic structure of the interface and, consequently, changes functional interface properties such as the height of the valence-band offset. The physics behind the valence-band offset is fairly well understood, at least for ideal tetrahedrally coordinated systems which show both atomic order and no interdiffusion.[9] For these ideal systems, one may also characterize the strain in the overlayer and estimate changes induced in the offset. These additional changes, of course, depend on the specific growth direction since strain is a directionally dependent quality.

We studied the atomic and electronic structure of CdS grown *in situ* on CdTe(110) substrates with angle-resolved synchrotron-radiation photoemission (ARPES) and reflection high-energy electron diffraction (RHEED). The CdS films were grown by molecular-beam epitaxy (MBE) on atomically clean and highly ordered CdTe(110). The microscopic evolution of the interface and the electronic properties were measured by surface-sensitive core-level and valence-band photoemission spectroscopy. Our experiments suggest that in addition to being a high-quality heterostructure suitable for use as a photovoltaic device, the special properties of the band

lineup across the heterostructure interface makes this system a potentially interesting candidate for type-I superlattice structures. The barrier heights for hole and electron confinement are $\Delta E_v = 0.65$ eV and $\Delta E_c = 0.21$ eV.

II. EXPERIMENT

The CdTe substrates used in the present investigation were platelets of 10×10 mm^2 with a thickness of 1 mm^2. The single-crystal wafers were oriented to within 2 sec of arc with respect to the surface normal along the (110) direction. The substrates, which were mechanically polished and chemically etched, were purchased from II-VI, Inc. in Saxonbourg, PA.

Advanced crystal growth and etching techniques resulted in a considerable narrowing of the double-crystal rocking curves (DCRC). The DCRC of the (400) reflections of the CdTe substrates showed a full width at half maximum of ~ 20 sec.[10] Prior to the film growth, the substrates were cleaned by Ar-ion sputtering. Several cleaning cycles, including sputtering with Ar ions of 500-eV kinetic energy and annealing for 5–10 min at ~ 280 °C, removed the surface oxide and reestablished crystal order. After the cleaning-annealing process the substrates showed a well-developed RHEED pattern.[11,12] Surface-sensitive *in situ* core-level spectroscopy confirmed that the CdTe surfaces were atomically clean.[12]

A single liquid nitrogen shrouded boron nitride effusion cell was the source of the deposited CdS films. Deposition rates, which were monitored with a calibrated water cooled quartz crystal thickness monitor, showed the typical Arrhenius behavior (logarithm of deposition rate is linear versus the reciprocal of the absolute source temperature). The measured growth rate indicates that a single effusion cell can release stoichiometric amounts of CdS in a certain temperature range and can be used as a molecular beam source for epitaxial growth.

Photoemission experiments were performed *in situ* using synchrotron radiation from the University of Wisconsin's 1-GeV electron storage ring Aladdin. A 2 m grazing incidence "Grasshopper" beamline provided monochromatic photons in the energy range $h\nu = 40$–140 eV. The total-energy resolution of the combined monochromator-spectrometer system was $\Delta E \sim 0.21$ eV at the lower photon energy side, and increased to ~ 0.4 eV at the higher-energy side of the available photon spectrum. Unless otherwise quoted, all binding energies are referenced with respect to the Fermi level. Binding energies are determined with an estimated accuracy of $\delta E_B \sim \pm 50$ meV. Considering these errors in the absolute binding energies, all experimental values which are based on energy differences (such as $\Delta\varepsilon_{VB}$) have an uncertainty of at least ± 70 meV.

III. RESULTS AND DISCUSSION

A. Experimental interface studies

The RHEED pattern of CdS grown at 250 °C on CdTe(110), which we discussed in a preliminary growth study, shows features typical for an ordered (110) zinc-blende surface.[12] In addition to the bright RHEED streaks, one can see higher-order diffraction spots which are distributed over a ring. Most important to note is that the deposition of CdS on the CdTe substrate does not change the principle structure and the spacing of the RHEED pattern. The persistency of the RHEED pattern is very strong evidence for the epitaxial growth of cubic CdS, in registry with the underlying substrate. The absence of additional spots rules out the possibility of other phases. A closer look at the RHEED pattern shows that even though the principle structure remains constant, the background intensity enhances slightly with increasing overlayer thickness. The rise in background intensity is most likely related to the accumulation of misfit dislocations.

Figure 1 is a plot of the intensity of the Te 4*d* core-level emission as a function of the thickness of the CdS overlayer film. For a two-dimensional layer-by-layer growth mode, one expects the substrate core-level intensity to decrease exponentially (e.g., linear when plotted on a semilogarithmic scale). The circles and squares are experimental points for growth temperatures $T_{sub} = 25$ and 250°C. The line is a fit to the experimental data points. In both cases, the kinetic energy of the outcoming electrons is ~ 55 eV, which is near the minimum in the universal escape depth curve. The points clearly follow the behavior expected for an epitaxial layer by layer

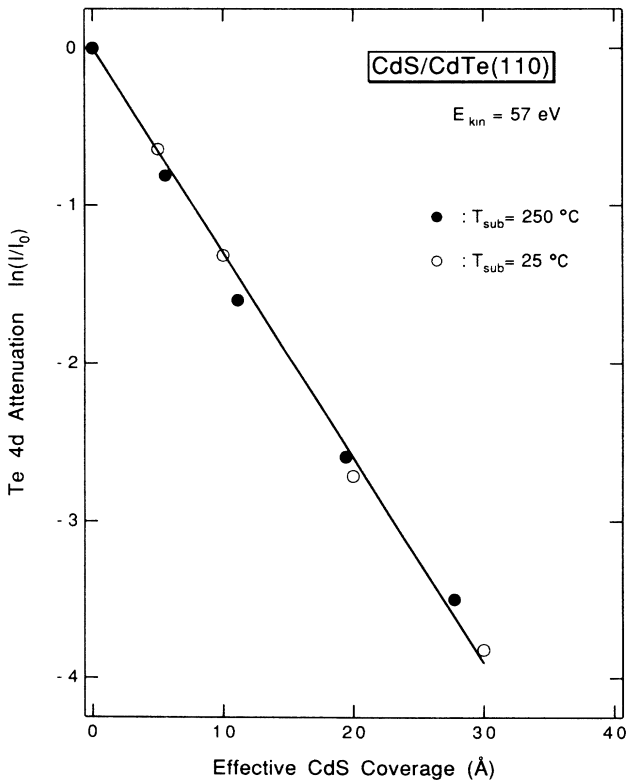

FIG. 1. Normalized Te 4*d* substrate intensity as a function of nominal CdS overlayer thickness.

growth. Since the substrate surface provides the proper cation and anion bonding pattern, the CdS/CdTe(110) system does not exhibit the phase and boundary domain problems seen during the initial stages of the epitaxial growth of CdTe on a neutral diamond structured α-Sn(110) surface.[13]

Since the substrate emission attenuates like $\ln(I/I_0) = -d/\lambda_{el}$, where d is the thickness of the overlayer and λ_{el} is the escape depth of the photoemitted electrons, the escape depth is simply determined by the slope of the attenuation curve. From Fig. 1, we obtain an escape depth of $\lambda_{el}=9$ Å for photoelectrons of kinetic energy $E_{kin}\sim 57$ eV. The experimentally determined escape depth is reasonable when compared with the universal escape depth curve and data from other semiconductor materials.[14–16]

It should be mentioned that the raw data points (solid circles) representing the CdS deposition at a substrate temperature of $T_{sub}=250$ °C actually show a much smaller attenuation resulting from a temperature-induced decrease in the sticking coefficient. We measured a larger escape depth of $\lambda_{el}=72$ Å, if the Te 4d intensity is plotted against the nominal CdS coverage as measured with the water cooled quartz monitor. As we will show later, the discrepancy between attenuation curves obtained at 250 °C and at room-temperature deposition does not indicate that the interface is reactive and nonabrupt. The apparent inconsistency in the electron mean free path of these two films can be explained by a reduced sticking probability η for CdS deposited at elevated substrate temperatures. Postulating a unit sticking coefficient at room temperature, the high-temperature attenuation curve suggests a reduction of the sticking probability to $\eta_{250\,°C}\sim 0.14$. Considering the temperature dependence of the sticking probability, we determine the effective film thickness to be $d_{eff}=\eta_{250\,°C}d_{nom}$.

The consistency of the line shape of the Te 4d spectra with increasing CdS coverage also argues strongly in favor of an abrupt CdS/CdTe interface. Figure 2 displays the Te 4d core-level emission as a function of CdS films deposited at room temperature. For growth at 250 °C we find the same spectral response. With increasing CdS film thickness, one sees neither a change in the binding energy nor the presence of additional components. Even though the spectrum for the 10-Å film suggests a decrease in binding energy by $\Delta E_B\sim 0.1$ eV, we do not consider this to be a real effect, since other spectra for thinner films do not indicate the same trend.

In contrast to the Te 4d core spectra, the Cd 4d emission shows a considerable shift to higher binding energy. Figure 3 shows a set of Cd 4d core spectra as a function of CdS coverage. The binding energy in CdS is $E_B(4d_{5/2})=10.45$ eV as compared to 10.05 eV in the CdTe. Assigning the change in binding energy to a larger positive charge for Cd in CdS than in CdTe is difficult, since no clear definition of atomic charge in semiconductors exists. In tight-binding theory, one uses the polarity of the bonds to determine the charge on the atoms via the equation $Z^*=Z-4+4\alpha_p$. This approach leads to effective Cd charges of $Z^*_{CdS}=+0.776e$ and $Z^*_{CdTe}=+0.624e$.[17,18] Since Cd is somewhat more positively

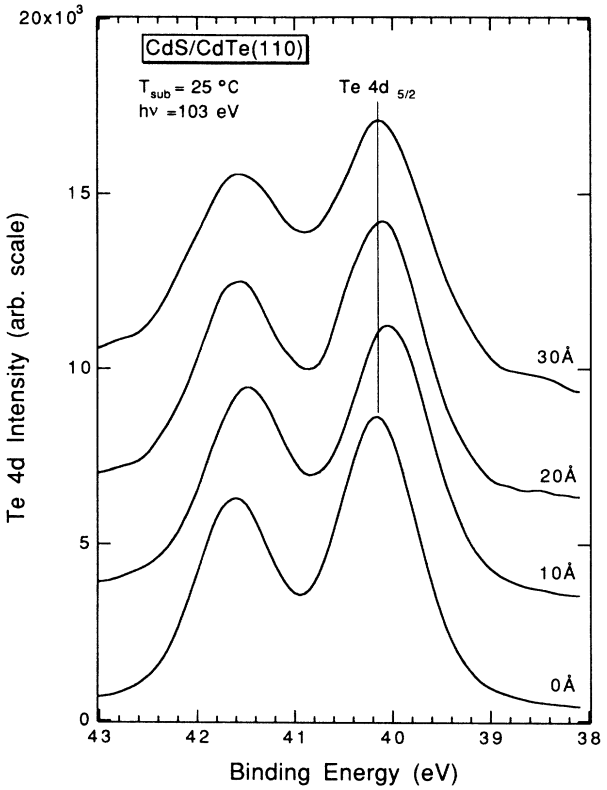

FIG. 2. Te 4d core spectra as a function of CdS film thickness deposited on CdTe(110) at ~25°C. The spectra were taken at normal emission with a photon energy of $h\nu=103$ eV.

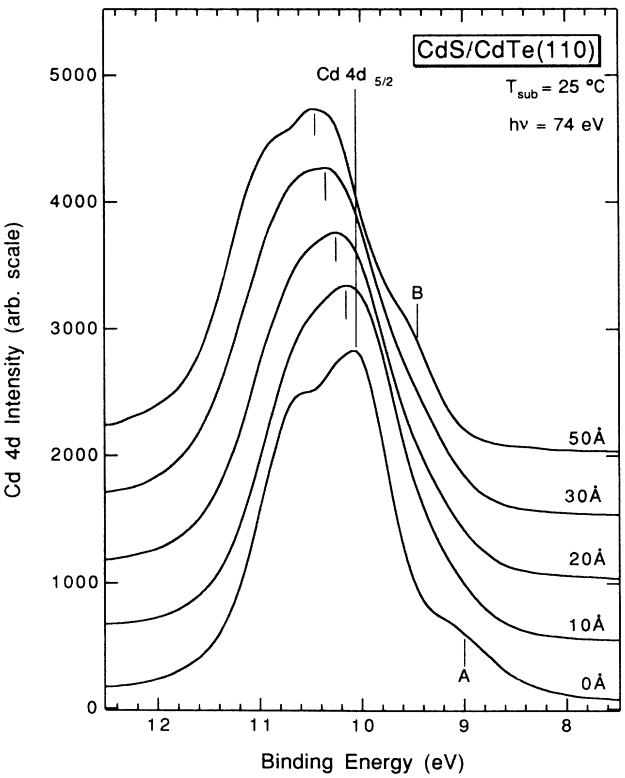

FIG. 3. Cd 4d core-level emission as a function of CdS overlayer thickness. The spectra were measured at normal emission with a photon energy of $h\nu=74$ eV.

charged in CdS than in CdTe, Cd 4*d* core-level binding energies should be slightly higher in CdS, in agreement with the observation. Increasing the bond length in accordance with tensile strain decreases the difference in effective charges. The same trend is predicted by more-recent calculations considering bond polarities.[19]

For intermediate CdS film thicknesses, the Cd 4*d* line shape can be simulated by a superposition of the spectra of clean CdTe and that of a 50-Å-thick CdS film. Using weighting factors for these two spectra according to the attenuation behavior shown in Fig. 1, we obtain a theoretical spectrum of the CdS/CdTe interface which is shown in Fig. 4. The quality of the simulation is quite good, except for a small region centered around $E_B = 8.7$ eV. This region of poor fit, however, contains additional fine structure, which we will discuss shortly.

Deposition at $T_{sub} = 250\,^{\circ}C$ shows essentially the same nonreactive two-dimensional growth behavior. The only minor difference is the appearance of a weak shoulder *A* in the Cd 4*d* spectra at ~0.85 eV below the $4d_{5/2}$ emission. This shoulder which is labeled *B* in Fig. 3 is also visible, but less pronounced, for CdS films deposited at 25 °C. The appearance of this additional feature is clearly linked to improved structural quality of the CdS film grown at higher substrate temperature, but its origin is yet unclear. A similar spectral feature is present in CdSe,[20] cleaved hexagonal CdS,[21] and CdTe.[22,23] It may be due to a hybridization between the Cd 4*d* and S 3*s* states as suggested in a theoretical study,[24] or it may be a joint density of states feature from the lowest occupied valence band, as assigned in a recent angle-resolved study of CdTe(110).[23]

A complete analysis would also cover the S 2*p* core-level emission from the overlayer. Unfortunately the binding energy of that level is too deep in energy to be reached with photons available in our present study.

Figure 5 shows the normal emission valence-band spectra of the interface as a function of the effective CdS coverage. Despite being measured with a fairly small angular acceptance cone of $\Delta\theta \sim 2°$, the spectral features for excitation energies exceeding $h\nu = 70$ eV resemble mainly the density of states (DOS) of the occupied valence band, since the availability of final states is large. For instance, the peak labeled *A* which is characteristic for CdTe corresponds to emission from the flat parts of the third valence band near the *L*, *X*, *K*, and *W* points.[24–26] Depositing CdS on top of CdTe attenuates this feature while a new structure labeled *B* increases. Peak *B* corresponds to emission from the same flat regions in the third valence-band regions of cubic CdS. Since the Cd 4*d* and

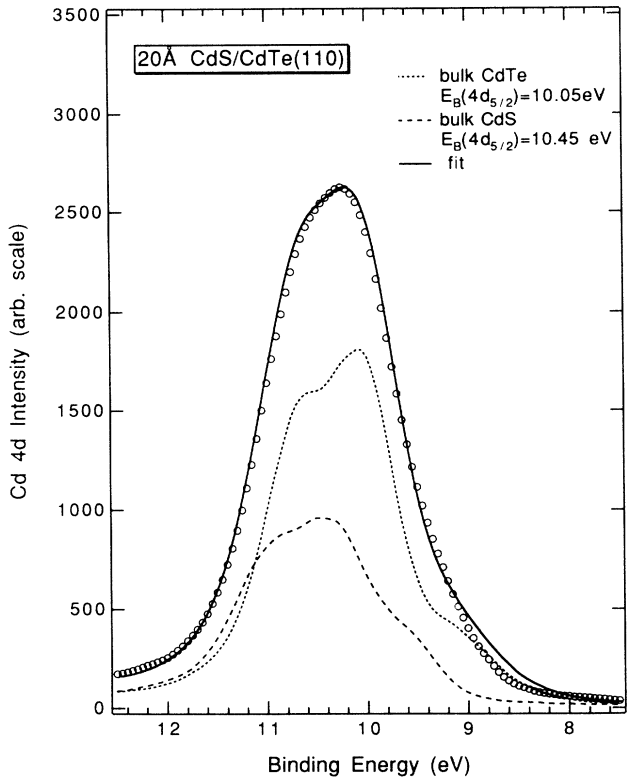

FIG. 4. Cd 4*d* core-level emission line shape for a 20-Å CdS film on CdTe(110), decomposed into CdS and CdTe components as described in the text.

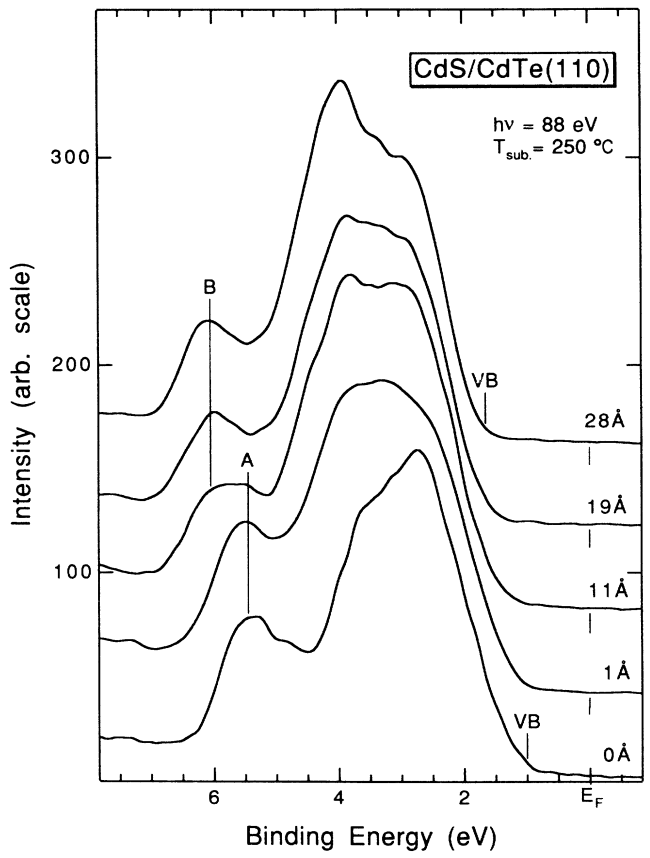

FIG. 5. Normal-emission valence-band spectra of the CdS/CdTe(110) interface as a function of CdS overlayer thickness.

Te 4*d* core spectra do not show shifts associated with changes in band bending, we take the surface Fermi level position to be constant and independent of CdS coverage. As one can see by comparing the top and the bottom spectra, intermediate spectra are a mixture of the two endpoints. They can be simulated in the same way as described for the Cd 4*d* core-level emission by a weighted superposition of CdS and CdTe valence-band spectra.

The top of the valence band of CdTe, as previously determined by an angular resolved study of CdTe(110), is indicated by VB in Fig. 5.[23] To find the VB for CdS, one can compare the measured EDC (electron distribution curve) to a DOS calculation, as shown in Fig. 6. Here we plot the measured EDC taken from Fig. 5 with the theoretical DOS taken from the band-structure calculation of Zunger and Freeman.[25] One should note that the CdS DOS has not been convoluted to consider broadenings due to the limited experimental resolution and lifetime effects of the photohole. Inclusion of an energy-dependent lifetime broadening would diminish the intensity of the higher-binding-energy features in the DOS with respect to those of the region near the valence-band maximum.[27,28] Even though considering some sort of a lifetime variation across the width of the valence band would certainly help to improve the overall agreement with our experimental valence-band spectrum, we did not attempt to fit these additional parameters. For the purpose of the present paper, where we are mainly concerned with identifying the position of the top of the valence band, such effects are of minor importance. As one can see from Fig. 6, the position of the calculated VB is in good agreement with the measured valence-band spectrum. To emphasize the differences between the valence-band EDC's of the phases of CdS, Fig. 6 also displays the photoemission spectrum of hexagonal CdS.[29]

After ruling out band bending changes and determining the valence-band maxima for the substrate and the overlayer, one can estimate the valence-band offset directly from Fig. 5 by taking the difference $\varepsilon_{VB(CdTe)}-\varepsilon_{VB(CdS)}$. We find $\Delta\varepsilon_{VB}=-0.65$ eV. Using E_g(CdS)=2.42 eV and E_g(CdTe)=1.56 eV gives $\Delta\varepsilon_{CB}=0.21$ eV. A band diagram of the experimentally determined band lineup across the CdS/CdTe interface is given in Fig. 7.

B. Theoretical considerations of the CdS/CdTe interface

The dominant effect controlling the alignment of semiconductors at an ideal interface is a transfer of charge which forces the dielectric midgap energies of the two components to align.[30] Although detailed calculations have been performed for many pairs of semiconductors, no theoretical results exist for the CdS/CdTe system. In

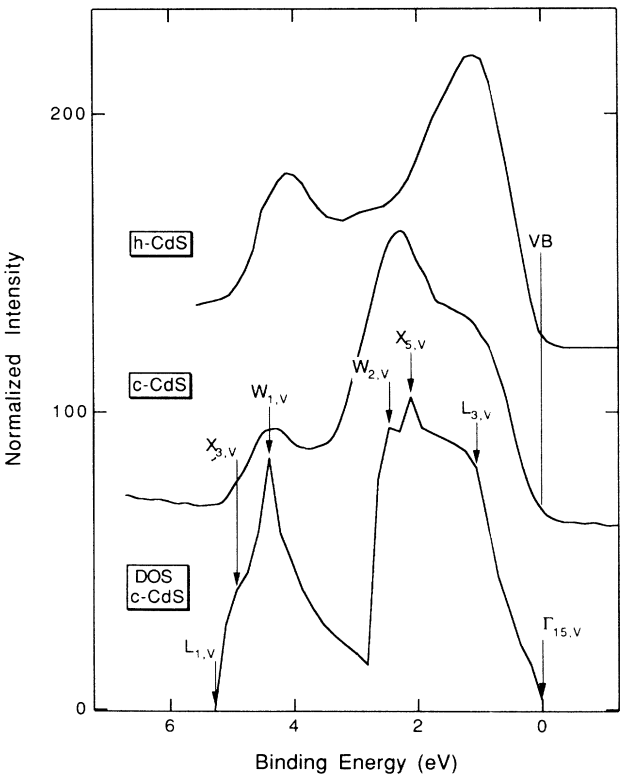

FIG. 6. Comparison between the calculated DOS of cubic CdS (from Ref. 26) with the measured valence-band spectrum of an epitaxial CdS, used to determine the valence-band maximum for CdS. Also shown is the EDC of hexagonal CdS (from Ref. 30).

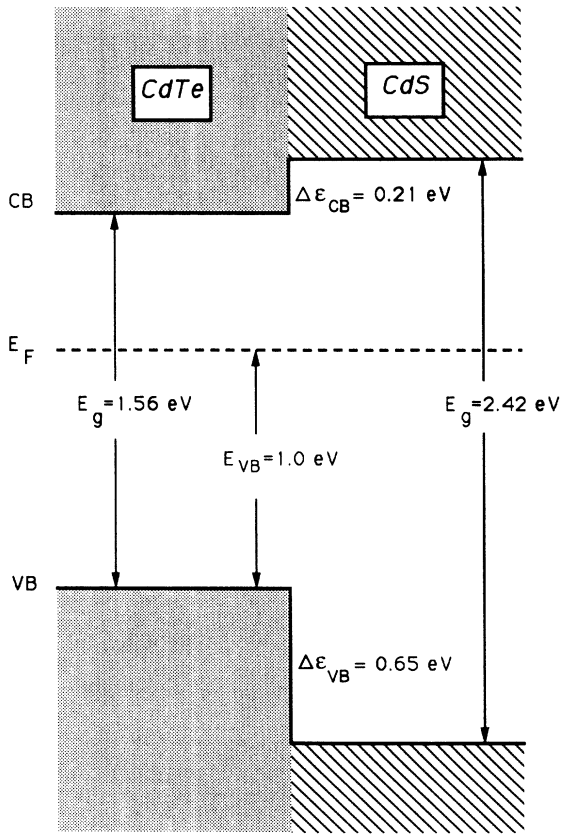

FIG. 7. Schematic of the experimentally determined band lineup across the CdS/CdTe(110) heterojunction.

lieu of these, one may use tight-binding theory, where the dielectric midgap energy is given by the average sp^3 hybrid energy.[31] The expression for the band offset is

$$\Delta\varepsilon_{VB}=(\varepsilon_{h1}-\varepsilon_{v1})-(\varepsilon_{h2}-\varepsilon_{v2})-(\varepsilon_{h1}-\varepsilon_{h2})/\epsilon_\infty \ , \quad (1)$$

where ε_h is the energy of the sp^3 hybrid, ε_v is the valence-band maximum, and ϵ_∞ is the average interface dielectric constant at infinite wavelength.[32] Take note of the limits of Eq (1). For a perfect dielectric response, one sets $\epsilon_\infty=\infty$, leading to align the sp^3 hybrid energies across the junction. For a system with no dielectric response one sets $\epsilon_\infty=1$, recovering the familiar electron affinity rule. Since ϵ_∞ is usually near 10, the dominant effect is the alignment of the hybrids.

The energy of the average sp^3 hybrid state for a polar semiconductor is given by

$$\varepsilon_h=[3(\varepsilon_p^a+\varepsilon_p^c)+(\varepsilon_s^a+\varepsilon_s^c)]/8 \ , \quad (2)$$

where $\varepsilon_p^{a,c}$ and $\varepsilon_s^{a,c}$ are the anion and cation p- and s-state energy levels.[17] For a cubic semiconductor with T_d point symmetry, the valence-band maximum is the triply degenerate (excluding spin degeneracy) Γ_4 level, comprised solely of atomic p states. The atomiclike s states make up the nondegenerate Γ_1 state. This ignores spin-orbit coupling. The expression for the energy of the Γ_4 state, derived from Refs. 17 and 18, is

$$\varepsilon_{\Gamma_4}=(\varepsilon_p^c+\varepsilon_p^a)/2-\{[(\varepsilon_p^c-\varepsilon_p^a)/2]^2+[(1.28\hbar^2)/md^2]^2\}^{1/2} \ . \quad (3)$$

The inclusion of the spin-orbit coupling splits the threefold-degenerate Γ_4 state into a twofold-degenerate Γ_8 state and nondegenerate Γ_7 state. The Γ_8 state is higher in energy than the Γ_4 state by one third the spin-orbit splitting. The Γ_8 point represents the valence-band maximum, which is given by

$$\varepsilon_v=\varepsilon_{\Gamma_8}=\varepsilon_{\Gamma_4}+|\Delta\varepsilon_{s.o.}|/3 \ . \quad (4)$$

The plus sign is because ε_{Γ_4} is inherently a negative number, since the zero of energy is the vacuum level. Using Eqs. (1)–(4) and the value of Hartree-Fock terms from Ref. 18 allows us to calculate the valence-band offset

$$\Delta\varepsilon_{VB}=[\varepsilon_h(\mathrm{CdS})-\varepsilon_{\Gamma_8}(\mathrm{CdS})]-[\varepsilon_h(\mathrm{CdTe})-\varepsilon_{\Gamma_8}(\mathrm{CdTe})]-\frac{[\varepsilon_h(\mathrm{CdS})-\varepsilon_h(\mathrm{CdTe})]}{[\epsilon_\infty(\mathrm{CdS})+\epsilon_\infty(\mathrm{CdTe})]/2} \ . \quad (5)$$

The calculated valence-band offset along with the set of relevant parameters are given in Table I. The calculated offset for the unstrained CdS/CdTe interface is $\Delta\varepsilon_{VB}=1.21$ eV, which is much larger than our experimental value of 0.65 eV. Discrepancies between experiment and theoretical predictions based on the tight-binding approach generally agree within 0.2–0.3 eV, but are somewhat worse for the II-VI compounds.[31] Since we can expect an uncertainty of ~0.4 eV in the theoretical value, we conclude that experiment and theoretical predictions agree within the inherent theoretical uncertainties. However, CdS is highly strained, which may bring theoretical and experimental values closer together or may separate them so that they no longer overlap.

Detailed calculations of the strain dependence of the band offsets are not straightforward. The hydrostatic part of the strain can easily be dealt with by estimating volume deformation potentials from Eqs. (2) and (3), but the shear component is much less tractable. For our present study, the shear component which accompanies growth along the (011) direction reduces the symmetry of cubic CdS from T_d to C_{2v}. Since the C_{2v} point group has no degenerate representations, the strain has completely removed all degeneracies and the Γ_8 valence-band maximum splits into two levels. Furthermore, the assignment of the hybrid energy level as the dielectric midgap energy is no longer obvious, since the 24 Baldereschi points of the T_d point group split into six groups of 4 in the C_{2v} point group.

TABLE I. Parameters used to calculate the valence-band offset $\Delta\varepsilon_{VB}$ between cubic CdS and CdTe. The offset has been calculated considering a strain-free CdS overlayer ($\delta=0$) as well as for a CdS film which grows in lateral registry on CdTe under a tensile strain of $\delta=0.11$. The last column considers the case of full hydrostatic strain assuming $c_{44}\to\infty$.

	d (Å)	ε_H (eV)	ε_{Γ_4} (eV)	ε_{Γ_8} (eV)	$\Delta\varepsilon_{s.o.}$ (eV)	ϵ_∞	$\Delta\varepsilon_{VB}$ (eV)
CdTe	2.81	−8.365	−9.803	−9.499	0.91	7.2	0
CdS ($\delta=0$)	2.53	−9.750	−11.894	−11.870	0.07	5.2	1.210
CdS ($\delta=0.11$)	2.62[a]	−9.952	−12.060	−12.038	0.07	5.2	1.208
CdS ($\delta=0.11$) $c_{44}\to\infty$	2.81	−10.244	−12.291	−12.268	0.07	5.2	1.193

[a]Average bond length.

To keep in tune with the tight-binding estimate of the valence-band offset, we will estimate strain-induced changes by making use of the expressions for ε_{Γ_4} and ε_H. Strain will cause a change in both energy levels. Strictly speaking, the spin-orbit splitting depends on the lattice constant through the polarity, but this dependence is small since most of the charge is on the anion regardless of the degree of strain. On the contrary, ε_{Γ_4} depends strongly on the actual crystal properties through the bond length d. In order to compute the effect of strain, we must first calculate a new bond length, and then the corresponding energy position of ε_{Γ_4} to revise Table I. The band offset under the action of strain will be calculated by using Eq. (5) as we did before.

Since the lattice constant of unstrained CdS is $\sim 11\%$ smaller than that of CdTe, the CdS epilayer is under severe tensile strain in the plane of growth. This extension along the surface forces a contraction perpendicular to the surface, as depicted in Fig. 8, where we show a view of an (011) oriented overlayer as seen from the (100) direction. The open circles indicate the corners of the units cells for an unstrained overlayer, whereas the solid circles mark those for an overlayer under tensile strain. The natural lattice constant is a_0, and $\delta=(a-a_0)/a_0$ is the strain enforced by epitaxial growth on a substrate with lattice constant a.

Due to symmetry, the nonzero components of the overlayer strain tensor are $\varepsilon_1=\delta$, $\varepsilon_2=\varepsilon_3$, and ε_4. All other components are zero. Here we use Nye's notation.[33] From the inset of Fig. 8 one may derive that

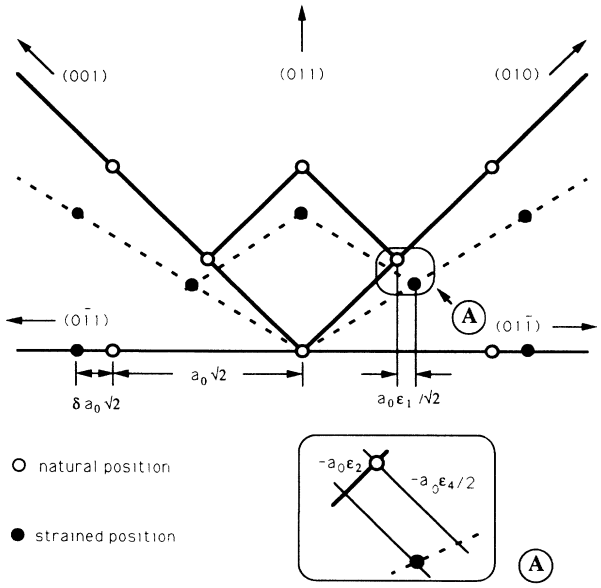

FIG. 8. View of a (011) grown overlayer seen from the (100) direction. Open circles mark the positions of atoms at the corners of the unstrained overlayer, while the solid circles represent the new positions for the epitaxial strained overlayer.

$$-\varepsilon_4/2=\varepsilon_1-\varepsilon_2 . \tag{6}$$

A further constraint in the overlayer is that the stress along the (011) direction is zero, and therefore $\sigma_2+\sigma_4=\sigma_3+\sigma_4=0$. Through use of the elastic constants, this last constraint becomes

$$c_{12}\varepsilon_1+(c_{11}+c_{12})\varepsilon_2+c_{44}\varepsilon_4=0 . \tag{7}$$

Combining these equations yields

$$\varepsilon_1=\delta , \tag{8}$$

$$\varepsilon_2=(2c_{44}-c_{12})\delta/(c_{11}+c_{12}+2c_{44}) , \tag{9}$$

$$\varepsilon_4=-2(c_{11}+2c_{12})\delta/(c_{11}+c_{12}+2c_{44}) . \tag{10}$$

The contraction along the (011) direction is given by

$$\alpha=[2(\varepsilon_4^2/4+\varepsilon_2^2)-\varepsilon_1^2]^{1/2} . \tag{11}$$

The elastic constants of CdS are $c_{11}=7.8$, $c_{12}=5.3$, and $c_{44}=2.4$.[34] Taking these modules and considering the difference between the lattice constants of cubic CdS and CdTe, we obtain the strain $\delta=0.11$ and $\varepsilon_1=0.11$, $\varepsilon_2=0$, $\varepsilon_4=-0.23$.

Through the strain the atomic positions are changed to

$$U_i=(U_0)_i+\sum_{j=1}^{3}\varepsilon_{ij}(U_0)_j , \tag{12}$$

where U_0 represents the positions for the unstrained lattice with $\varepsilon_{ii}=\varepsilon_i$, and $\varepsilon_4/2=\varepsilon_{23}$, with similar relations for ε_{12} and ε_{13}. Assuming that a sulfur atom is located at the (0,0,0) position, Cd atoms will be located at (1,1,1), $(-1,1,-1)$, $(1,-1,-1)$, and $(-1,-1,1)$. From Eq. (12) and the previous estimate of the strain components, one can derive the new bond lengths to be 2.42 Å for Cd atoms at (1,1,1) and $(1,-1,-1)$ positions and 2.81 Å for those at $(-1,1,-1)$ and $(-1,-1,1)$. The fact that not all bonds will be of equal length was to be expected, since the crystal now has only C_{2v} and not the original T_d symmetry. The bonds whose length are 2.81 Å are, of course, those in the growth plane since they are forced to have the same bond length of the CdTe substrate.

To discuss the strain-related change of the valence-band offset, we choose to separate the strain tensor into hydrostatic (unit tensor) and shear (traceless tensor) components. The hydrostatic part describes the volume change of the unit cell without deformation, whereas the shear component describes the deformation at fixed volume.

The hydrostatic strain component δ_{hydro} does not change the symmetry, but does alter the bond length, and this will change the energy of the Γ_8 valence-band maximum. Using the elastic constants of CdTe we obtain

$$\begin{aligned}\delta_{\text{hydro}}&=\delta(c_{11}-c_{12}+6c_{44})/3(c_{11}+c_{12}+2c_{44})\\&=0.315\delta .\end{aligned} \tag{13}$$

Hydrostatic strain thus modifies the lattice constant to $a_0(1+0.315\delta)$. With an 11% lattice mismatch ($\delta=0.11$) between CdS and CdTe the strained lattice constant be-

comes $a_{str}=1.035a_0$. From the strained lattice constant one may also calculate the bond length under hydrostatic strain 2.53 Å$\times 1.035=2.62$ Å, which is the average between the previously determined 2.42- and 2.81-Å bond lengths.

Under equilibrium lattice conditions (unstrained) the total energy in a hybrid bond is at minimum. The bond energy ε_b can be expressed by

$$\varepsilon_b=\varepsilon_h-(V_2^2+V_3^2)^{1/2} . \quad (14)$$

The term ε_h, which contains the kinetic energy of the electrons, increases sharply (more positive) as the bond length d decreases. At equilibrium we have $\partial\varepsilon_b/\partial d=0$. Assuming that the polar energy $V_3=(\varepsilon_p^c-\varepsilon_p^a)/2$ is independent of d, we can then calculate the bond-length dependence of ε_h to be

$$\partial\varepsilon_h/\partial d=(-2V_2^2/d)/(V_2^2+V_3^2)^{1/2} . \quad (15)$$

With $V_2=3.32\hbar^2/md^2$ and the polar energy V_3 we obtain the strain-induced shift $\Delta\varepsilon_h=-5.87\,\Delta a/a_0=-0.202$. Equation (3) for the energy of the valence-band maximum can be written as

$$\varepsilon_{\Gamma_4}=\varepsilon_h+\Delta\varepsilon_h+(V_1^a+V_1^c)/2-\{V_3^2+[(1.28\hbar^2)/md^2]^2\}^{1/2} , \quad (16)$$

where $V_1^{a,c}$ is the metallic energy, which we also assume not to vary with bond length. Strain-induced modifications in ε_{Γ_4} appear thus through $\Delta\varepsilon_h$ and the d^{-2} dependence of the last term. With strain we have calculated the new parameters ε_h and ε_{Γ_4}, and a new valence-band offset $\Delta\varepsilon_{VB}=1.207$ eV. The parameters relevant for the strained overlayer are also listed in Table I.

As one can see from Table I, the hydrostatic part of the strain makes a negligible change in the valence-band offset, and the question is whether this finding can be considered to be the rule or if it is accidental. What happens in the case of the CdS/CdTe heterostructure is that the various changes brought about by the modified bond length worked in such a way as to nearly cancel one another. A closer look at the certain strain-induced components reveals that the compensational effect is not entirely an accident. Strain leads to a relatively large shift ($\sim$0.2 eV) in ε_h, but as can be seen in the previous equation the valence-band maximum tends to be shifted in the same direction and with the same rate. For this reason the terms $(\varepsilon_h-\varepsilon_{\Gamma_8})$ of Eq. (5) vary only little with strain by the term $(1.28\hbar^2)/md^2$.

What appears to be accidental is that the change in ε_{Γ_8} by the d^{-2} term is opposite in sign and approximately equal to the change in $[\varepsilon_h(\mathrm{CdS})-\varepsilon_h(\mathrm{CdTe})]$ of Eq. (5). One can show this by keeping the bond length in CdS at a fixed length of 2.53 Å while making a moderate decrease in the CdTe bond length. In this case the change in $[\varepsilon_h(\mathrm{CdS})-\varepsilon_h(\mathrm{CdTe})]$ and the change in $\varepsilon_{\Gamma_8}(\mathrm{CdTe})$ caused by the d^{-2} term to work together, and led to a noticeable decrease in the offset.

Up to this point, the analysis has ignored the effect of the shear component of the strain. As already mentioned, the shear component will split all energy levels, since the C_{2v} point has only nondegenerate representations. This will effect both ε_h and ε_{Γ_8}. Since we determined ε_{Γ_8} by comparing our measured spectrum to a DOS calculation, we have implicitly measured the average valence-band maximum of the shear strain split components. Therefore, we do not expect to be sensitive to the strain splitting of Γ_8, and do not need to modify its energy further.

What does change significantly is the appropriate dielectric midgap energy to align. Using the bond lengths 2.42 and 2.81 Å gives two new hybrid energies $\varepsilon_h=-9.652$ and -10.244 eV. One may similarly expect the dielectric midgap energy to split into components separated by as much as $10.24-9.65=0.6$ eV, and it is not completely clear which energy to align. To stay with the model one would expect to align the hybrid energy associated with the 2.42-Å bond length, since that is the bond that reaches across the interface. The 2.81-Å bond is parallel to the interface. Therefore, one may use $\varepsilon_h=-9.652$ eV and leave the other energy levels untouched, which increases the theoretical offset to $\sim$1.46 eV. This value would then be considerably off from the measured valence-band offset of 0.65 eV.

However, we should mention that there are a number of other things that we are currently investigating which could also contribute to the observed discrepancy. First, the strain in the CdS film may relax, giving rise to misfits which could alter the electronic structure at the interface. Second, we determined the valence-band maximum of CdS by comparing the measured valence-band EDC's to a DOS calculation, which may easily lead to uncertainties of $\sim$0.3 eV. We believe that the only convincing way to determine the VBM is to map the valence bands by angle-resolved photoemission and to directly identify the Γ_{4v} point from these measurements.[35]

Before ending this section, we would also like to mention a semiempirical method, which was suggested by Tersoff, for estimating band offsets.[36] The valence-band offset for CdS/CdTe may be estimated by the difference between measured Schottky barriers of Au/CdS and Au/CdTe structures. Using this method yields $\Delta\varepsilon_{VB}=1.65-0.68$ eV$=0.97$ eV.[36,37] However, it should be noted that this empirical method contains additional experimental uncertainties since metal overlayers deposited on semiconductor surfaces are often plagued with problems such as diffusion, clustering, and interfacial reactivity. These problems seem to be of particular importance for metal overlayers deposited on II-VI compounds. Nevertheless, using the empirical method based on the reported Schottky barriers gives a value which is in reasonable agreement with our experiment, even though the Schottky measurements were performed on hexagonal CdS while our data consider zinc-blende-structured CdS.

IV. CONCLUSIONS

Cubic CdS can be grown by heteroepitaxy on CdTe(110) substrates. Surface sensitive quantitative

core-level photoemission spectroscopy provides evidence for a two-dimensional layer by layer growth mode for CdS films of up to at least ~50 Å thickness. Even at elevated growth temperatures the interface appears to be abrupt and nonreactive.

The experimental valence-band offset is $\Delta\varepsilon_{VB}=0.65$ eV. From the tight-binding calculations based on the dielectric midgap model we predict a valence-band offset of $\Delta\varepsilon_{VB}=1.19$ eV for the unstrained CdS/CdTe interface. Including the effects of hydrostatic strain caused by ~11% lattice mismatch in the CdS film, we find a valence-band offset which is only slightly smaller than that of the unstrained CdS film.

The theoretical results infer that the hydrostatic strain component produces essentially no net change in the valence-band offset. However, simple considerations of the hybrid level suggest that shear components split the dielectric midgap energy into six levels whose total separation is ~0.6 eV. Without going into a detailed analysis considering the internal displacement of Cd and S atoms associated with the c_{44} strain component, it is difficult to predict which level aligns to ε_h (CdTe) of the substrate.

The analysis of the strain has brought forth some salient points with regard to the effect of strain on the heterojunction band offsets. In particular, both the hydrostatic and shear components of the strain may lead to significant changes in the band lineup, but the shear components of the strain will generally have a larger effect. This is because the Γ_{4v} has the tendency to follow the hybrid level, and the difference has only weak dependence on the bond length. Therefore, the change in lattice constant perpendicular to the interface, rather than parallel to it, appears to be more important for the strain-induced change in band lineup.

The nonreactive CdS/CdTe interface and the nested band-gap alignment makes this system a potential candidate for type-I superlattices with sufficiently high hole and well barriers of 0.65 and 0.21 eV.

Additional studies including different growth directions, the critical thickness for epitaxial growth of high-quality cubic zinc-blende CdS, and the ability to grow CdTe overlayers on cubic zinc-blende CdS are presently under way in our laboratories.

ACKNOWLEDGMENTS

This work was funded by the Innovative Science and Technology Program of the Strategic Defense Initiative Organization (SDIO-IST), U.S. Department of Defense, and managed by the Naval Research Laboratory (NRL) under Contract No. N00014-86-K-2022. The authors would like to thank M. A. Engelhardt and the staff of the Synchrotron Radiation Center for help with many of the technical aspects of the experiments. One of us (D.W.N.) would also like to thank the Alexander von Humboldt-Stiftung (Bonn, Germany) for financial support.

*Author to whom all correspondence should be addressed.

[1]Y. S. Tyan and E. A. Perez-Albuerne, *16th Photovoltaic Specialist Conference, IEEE Conference Proceedings* (IEEE, New York, 1982), p. 794.
[2]D. L. Feucht, J. Vac. Sci. Technol. **14**, 57 (1977).
[3]P. K. Raychaudhurt, J. Appl. Phys. **62**, 3025 (1987).
[4]T. L. Chu, S. S. Chu, and S. T. Ang, J. Appl. Phys. **64**, 1233 (1988).
[5]M. Cardona, M. Weinstein, and G. A. Wolff, Phys. Rev. **140**, A633 (1965).
[6]*Landolt-Börnstein Tables III/17b* (Springer-Verlag, Berlin, 1982).
[7]F. G. Smith, Am. Mineral. **40**, 649 (1957).
[8]R. W. G. Wyckoff, *Crystal Structure* (Wiley, New York, 1963), p. 110.
[9]J. Tersoff, in *Heterostructures: A Modern View of Band Discontinuities and Applications,* edited by G. Margaritondo and F. Capasso (North-Holland, Amsterdam, 1988).
[10]H. Höchst, M. A. Engelhardt, R. C. Bowman, Jr., and P. M. Adams, Semicond. Sci. Technol. (to be published).
[11]I. Hernández-Calderón, D. W. Niles, and H. Höchst, J. Vac. Sci. Tecnhol. A **6**, 1343 (1988).
[12]M. A. Engelhardt, D. W. Niles, and H. Höchst, J. Vac. Sci. Technol. A (to be published).
[13]H. Höchst, D. W. Niles, and I Hernández-Calderón, J. Vac. Sci. Technol. B **6**, 1219 (1988).
[14]I. Lindau and W. E. Spicer, J. Electron Spectrosc. Relat. Phenom. **3**, 409 (1974).
[15]H. Grant and W. Mönch, Surf. Sci. **105**, 217 (1981).
[16]M. Tang, D. W. Niles, I. Hernández-Calderón, and H. Höchst, Phys. Rev. B **36**, 3336 (1987).
[17]W. A. Harrison, *Electronic Structure and Properties of Solids* (Freeman, San Francisco, 1980).
[18]Hartree-Fock values taken from W. A. Harrison, Phys. Rev. B **24**, 5835 (1981).
[19]N. E. Christensen, S. Satpathy, and Z. Pawlowski, Phys. Rev. B **36**, 1032 (1987).
[20]C. F. Brucker and L. J. Brillson, J. Vac. Sci. Technol. **18**, 787 (1981).
[21]N. G. Stoffel, Phys. Rev. B **28**, 3306 (1983).
[22]N. J. Shevchik, T. J. Tejeda, D. W. Langer, and M. Cardona, Phys. Status Solidi B **60**, 326 (1973).
[23]H. Höchst, D. W. Niles, and I. Hernández-Calderón, Phys. Rev. B **40**, 8370 (1989).
[24]Su-Huai Wei and A. Zunger, Phys. Rev. B **35**, 2557 (1987).
[25]A. Zunger and A. Freeman, Phys. Rev. B **17**, 4850 (1978).
[26]K. J. Chang, S. Froyen, and M. L. Cohen, Phys. Rev. B **28**, 4736 (1983).
[27]H. Höchst, S. Hüfner, and A. Goldman, Phys. Lett. **57A**, 265 (1976).
[28]P. Thiry, D. Chandesris, J. Lecante, C. Guillot, R. Pinchaux, and Y. Petroff, Phys. Rev. Lett. **43**, 82 (1979).
[29]Spectrum of hexagonal CdS taken from D. W. Niles, Ph.D. thesis, University of Wisconsin–Madison (1988).
[30]M. Cardona and N. E. Christensen, Phys. Rev. B **35**, 6182 (1987) and references therein.

[31]W. A. Harrison and J. Tersoff, J. Vac. Sci. Technol. B **4**, 1068 (1986).
[32]W. A. Harrison and J. E. Klepeis, Phys. Rev. B **37**, 864 (1988).
[33]J. F. Nye, *Physical Properties of Crystals* (Clarendon, Oxford, 1969).
[34]R. M. Martin, Phys. Rev. B **6**, 4546 (1972).
[35]D. W. Niles and H. Höchst, Phys. Rev. B. **39**, 7769 (1989).
[36]J. Tersoff, Phys. Rev. Lett. **56**, 2755 (1986).
[37]L. Brillson, Phys. Rev. B **18**, 2431 (1978).

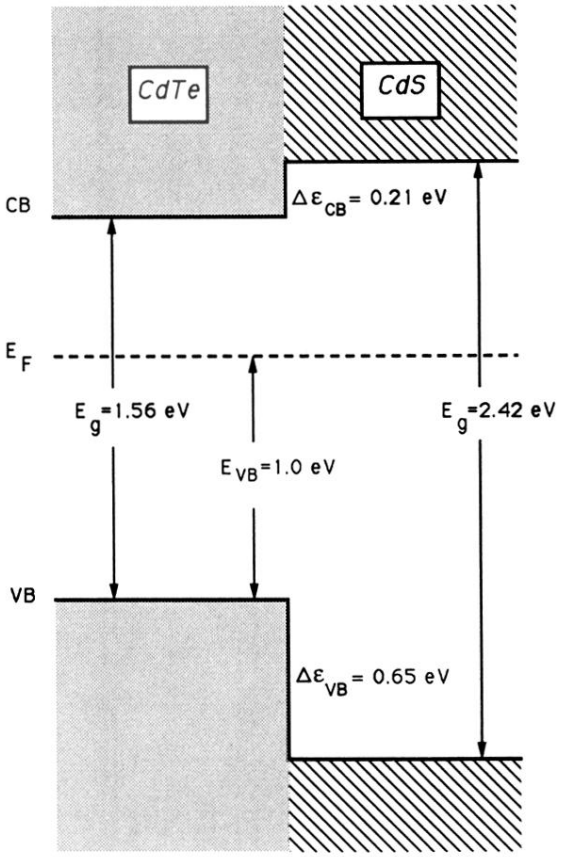

FIG. 7. Schematic of the experimentally determined band lineup across the CdS/CdTe(110) heterojunction.